Internal Model Control Design for Transition Control

Min-Sen Chiu and Shan Cui
Dept. of Chemical and Environmental Engineering, National University of Singapore, 10 Kent Ridge Crescent, Singapore 119260

Qing-Guo Wang
Dept. of Electrical Engineering, National University of Singapore, 10 Kent Ridge Crescent, Singapore 119260

The problem of controlling processes with a wide range of operating conditions is addressed. The process dynamics is represented by the weighted-sum of the linear model by using model validity functions. By treating the validity functions as uncertainties in the system, an internal model control (IMC) design strategy is developed for a particular class of nonlinear systems. Robust stability analysis under mixed time-varying and time-invariant uncertainties is presented. Simulation results confirm that the proposed IMC design method is indeed superior to its conventional counterpart.

Introduction

Traditionally, model-based control strategies for chemical processes are to design a linear controller based on the linearized model. For open-loop stable systems, internal model control (IMC) provides a convenient parametrization of all stabilizing controllers (Morari and Zafiriou, 1989). In fact, under the perfect model assumption, closed-loop stability becomes a trivial task using the design of a stable IMC controller. When the plant/model mismatch occurs, an IMC filter can be used to make a compromise between the robustness and performance requirement. Although most chemical processes are nonlinear in nature, the IMC controller is able to perform satisfactorily as long as the plant is operated in the vicinity of the point where the linearization is generated. When the plant is to be operated over a wide range of operating conditions, as a consequence of large setpoint changes and/or the presence of disturbances, the H^∞ robust control framework can be employed to design an IMC controller. One possible way is to treat the local model of one operating point as the nominal model and those in the rest of operating region as the perturbed models. Consequently, a robust IMC design can be obtained if the corresponding H^∞ design criterion can be met (Morari and Zafiriou, 1989). However, due to the worst-case design concept employed in the H^∞ design, the resultant IMC controller can be conservative and is not able to achieve the desired performance in the operating region considered.

The objective of this article is to propose a novel IMC design to address this control problem. To do so, the concept of operating region decomposition is applied to decompose a dynamic system into a set of operating regimes (Takagi and Sugeno, 1985; Pottmann et al., 1993; Johansen and Foss, 1993, 1997; Feng et al., 1996; Banerjee et al., 1997; Palizban et al., 1997) In addition, various functions were employed in these works to calculate the model validity function, which is associated with each of the local models. It is then assumed that the weighted-sum of the local models using the model validity function can describe the dynamics of a certain class of nonlinear systems. This modeling approach is commonly termed local model networks or multiple model in the literature.

In this article, the particular structure of local model selected is the transfer-function model, which can be obtained from either linearization of first-principles model or identification from available input–output data. Under perfect-model assumption, the global multiple model is employed to represent the actual process dynamics in the IMC structure, and the main goal of this article is to analyze the associated nominal performance in the H^∞ control framework. It is shown that the model validity functions can be treated as

Correspondence concerning this article should be addressed to M.-S. Chiu.

time-varying uncertainties, and the resulting robust control problem is solved by employing the structured singular value test for mixed time-varying and time-invariant perturbations (Paganini, 1996). A continuous stirred-tank reactor and a fermentor are used to illustrate the proposed IMC design method, and a comparison with the conventional IMC design is made.

Global Multiple Model

In system identification, it may be possible to model accurately the process dynamics over the entire range of operating conditions using a single highly nonlinear model. However, nonlinear model building is a cumbersome task. Besides, it will most likely complicate the subsequent controller design. Thus, this modeling approach is not an attractive alternative. A promising approach is to decompose the system's operating space Γ into n operating regimes Γ_i, which cover the relevant range of operations. Subsequently, simple local model structures are developed for each regime and the global multiple model is formed by connecting the set of local models by model validity function.

Several local model structures, including state-space model (Feng et al., 1996; Banerjee et al., 1997), polynomial model (Takagi and Sugeno, 1985; Pottmann et al., 1993), ARX model (Johansen and Foss, 1997), and ARMAX model (Johansen and Foss, 1993; Palizban et al., 1997), have been employed in previous studies on modeling using the multiple model. In this article, a transfer-function model is used to describe the process dynamics in each operating regime Γ_i. For a single-input–single-output (SISO) stable nonlinear process, the ith local model has the following form:

$$Y_i(s) = G_i(s) \cdot U(s), \tag{1}$$

where $Y_i(s)$ and $U(s)$ are the Laplace transform of the output and input variable, respectively, and $G_i(s)$ is the transfer-function model.

For each local model there exists a weighting function to validate the local model. The value of the model validity function γ_i depends on states, inputs and outputs of the process, and is bounded between zero and one. Generally, its value is close to one for the operating regime where the local model $G_i(s)$ is a good description of the system; otherwise it is close to zero. Regardless of various algorithms used to calculate γ_i, it has the following property:

$$\sum_{i=1}^{n} \gamma_i = 1. \tag{2}$$

Thus, the global multiple model is represented as

$$Y(s) = \sum_{i=1}^{n} \gamma_i Y_i(s) = G(\gamma) \cdot U(s), \tag{3}$$

where $\gamma = (\gamma_1, \gamma_2, \ldots, \gamma_n)$ and

$$G(\gamma) = \sum_{i=1}^{n} \gamma_i G_i(s). \tag{4}$$

It is clear that the global model is a weighted sum of the local models and there is at least one nonzero model validity function at any operating point.

In what follows, the advantage of using Eq. 4 in modeling a dynamic system with a range of operating points is analyzed. Specifically, it will be shown that for a given set of local models, the uncertainty modeling used in the H^∞ control framework admits a larger class of possible plants.

In the H^∞ control design, the common practice is to choose one local model as the nominal model denoted by G_M, and the information on the rest of local models can be used to determine the uncertainty weighting function, without loss of generality, in multiplicative uncertainty description:

$$G = G_M(1 + l_1\Delta_I), \quad G \in \{G_1, G_2, \ldots, G_n\}, \quad |\Delta_I| < 1, \quad \forall\omega. \tag{5}$$

For comparison, the global multiple model is also put in the uncertainty description from

$$G(\gamma) = G_M(1 + l_2\Delta_I), \qquad |\Delta_I| < 1, \quad \forall\omega. \tag{6}$$

The following theorem summarizes the overbounding result of Eq. 5.

Theorem 1. Given a set of local models of a dynamic system operated over a range of operating conditions and two uncertainty descriptions given in Eqs. 5 and 6, the following relation holds:

$$|l_2| \le |l_1| \qquad \forall\omega. \tag{7}$$

Proof. See Appendix A.

The implication of Theorem 1 is that a conservative controller design may result from the overbounding effect of Eq. 5. As a result, the control system cannot achieve the desired performance in the entire operating space considered, as will be demonstrated in the following examples.

H^∞ Analysis of IMC Control Structure Using Multiple Models

In this section, an analytical framework will be devised for the H^∞ control of IMC structure where the actual process is represented by the global model of Eq. 4. Figure 1 depicts this IMC structure, where G_M can be any one of the local models and is the nominal model used in the design of con-

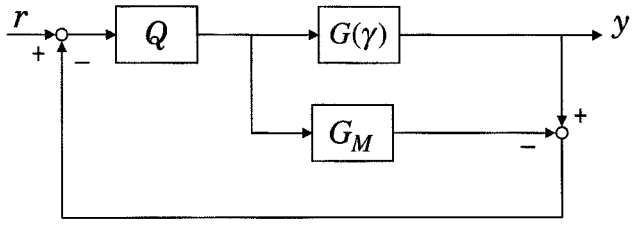

Figure 1. Multiple-model-based IMC structure.

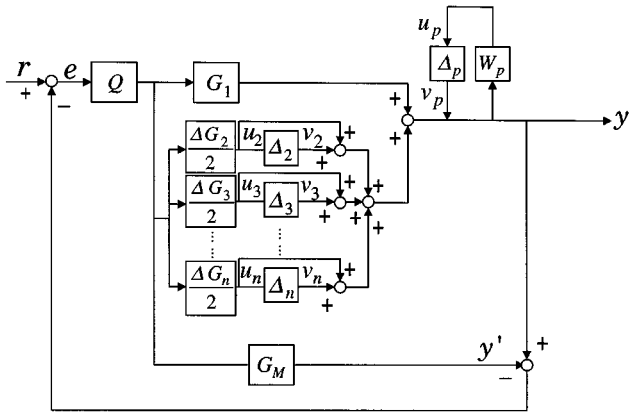

Figure 2. Multiple-model-based IMC structure with H^∞ performance specification.

ventional IMC controller Q as follows:

$$Q = \frac{1}{(\epsilon s + 1)^r} \cdot \frac{1}{G_{M_-}}, \tag{8}$$

where G_{M_-} is the minimum phase of G_M; ϵ is the IMC filter time constant, which can be adjusted to satisfy the performance requirement; and r the order of the IMC filter.

We are now ready to analyze the H^∞ performance of this IMC system. Because of Eq. 2, the expression of $G(\gamma_i)$ can be rewritten as

$$G(\gamma) = G_1 + \sum_{i=2}^{n} \gamma_i (G_i - G_1) = G_1 + \sum_{i=2}^{n} \gamma_i \Delta G_i. \tag{9}$$

Next, the validity function γ_i is treated as an uncertainty, since γ_i can be rewritten as

$$\gamma_i = 0.5(1 + \Delta_i), \qquad |\Delta_i| \le 1 \quad i = 1, 2, \ldots, n. \tag{10}$$

Using the two preceding equations, Figure 1 is easily converted to Figure 2, where the additional Δ_p block represents H^∞ performance requirement and W_p is the performance weighting function. By simply reorganizing the diagram and collecting all of the perturbations together, we end up with the diagram in Figure 3, with

$$M = \frac{1}{1 + \left(G_1 - G_M + 0.5 \sum_{2}^{n} \Delta G_i \right) Q} \times \begin{bmatrix} -0.5\Delta G_2 Q & -0.5\Delta G_2 Q & \cdots & \cdots & -0.5\Delta G_2 Q \\ -0.5\Delta G_3 Q & -0.5\Delta G_3 Q & \cdots & \cdots & -0.5\Delta G_3 Q \\ \vdots & \vdots & \vdots & \vdots & \vdots \\ -0.5\Delta G_n Q & -0.5\Delta G_n Q & \cdots & \cdots & -0.5\Delta G_n Q \\ (1 - G_M Q) W_p & (1 - G_M Q) W_p & \cdots & \cdots & (1 - G_M Q) W_p \end{bmatrix} \tag{11}$$

$$\Delta = \begin{bmatrix} \Delta_2 & & & & \\ & \ddots & & & \\ & & \Delta_n & & \\ & & & \Delta_p & \end{bmatrix}, \qquad \| \Delta \|_\infty \le 1. \tag{12}$$

The derivation of the preceding equations is given in Appendix B.

As just mentioned, the local models are interpolated by model validity functions to form the global multiple model. Since the value of γ_i is dependent on the system dynamics, it is clear that perturbation Δ_i is time-varying in nature. Thus, the robust control problem shown in Figure 3 is to design an IMC controller Q such that for all allowable linear time-varying (LTV) perturbations Δ, the closed-loop system is stable. Note that Figure 3 is the standard setup for robust stability and performance analysis under structured uncertainty Δ, which has received a tremendous amount of research interest in the past two decades. When Δ contains only linear time-invariant (LTI) perturbation, Doyle (1982) developed a necessary and sufficient condition in terms of the structured singular value μ. However, if the block Δ includes some LTV perturbations, the conventional μ analysis may not give accurate results (Packard and Doyle, 1993). Recently, robustness analysis under LTV uncertainty has seen major progress (Shamma, 1994; Poola and Tikku, 1995; Paganini, 1996). In our view, the most interesting work is done by Paganini (1996), who proposed a μ test based on a finite augmentation of the original $M - \Delta$ structure as the necessary and sufficient condition for robustness analysis under structured uncertainties involving a combination of LTI and LTV uncertainties. To apply these results in our analysis, an augmented structure of the complex uncertainties is defined as follows:

$$\tilde{\Delta} = \left[\Delta_{ij} \right]_{i,j = 1,2, \ldots, n-1}, \tag{13}$$

where the diagonal entries are obtained simply by considering n copies of Δ. This means that Δ_{ii} has the identical

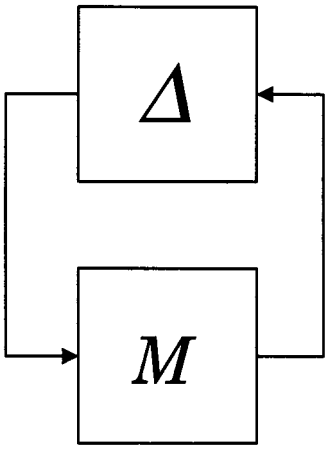

Figure 3. Interconnection structure.

structure of Δ, that is,

$$\Delta_{ii} = \text{diag}[\,\delta_k\,], \qquad |\delta_k| \le 1, \qquad i = 1,2,\ \ldots,\ n-1,$$
$$k = 1,\ 2,\ \ldots,\ n. \quad (14)$$

In a similar fashion, the off-diagonal uncertainty Δ_{ij} has the following structure

$$\Delta_{ij} = \begin{bmatrix} \delta_1 & & & & \\ & \delta_2 & & & \\ & & \ddots & & \\ & & & \delta_{n-1} & \\ & & & & 0 \end{bmatrix}, \qquad i,j = 1,2,\ \ldots,\ n-1,$$
$$i \ne j. \quad (15)$$

Obviously, the structure of $\tilde{\Delta}$ is $n-1$ times as large as the original Δ. The advantage of this augmentation, however, is to convert the original problem to one with LTI perturbations where the standard μ computation of Doyle (1982) can be applied straightforwardly. Having defined the uncertainty $\tilde{\Delta}$, the following theorem gives the IMC design criterion for a dynamic system, which can be described by the multiple model given in Eq. 4. The proof of the next theorem follows closely to that given in Paganini (1996) and thus is omitted here.

Theorem 2. Assume that the matrix M in Figure 3 is stable. The uncertain system in this diagram is robustly stable under mixed LTI and LTV uncertainties Δ if and only if

$$\max_{\omega_1,\ \ldots,\ \omega_{n-1}} \mu_{\tilde{\Delta}}\left(\tilde{M}(\omega_1,\ \ldots,\omega_{n-1})\right) < 1,$$
$$\omega_1,\ \ldots,\ \omega_{n-1} \in [0\ \infty), \quad (16)$$

where

$$\tilde{M}(\omega_1,\ \ldots,\ \omega_{n-1}) = \begin{bmatrix} M(j\omega_1) & & & \\ & M(j\omega_2) & & \\ & & \ddots & \\ & & & M(j\omega_{n-1}) \end{bmatrix}. \quad (17)$$

Note that the structure of $\tilde{\Delta}$ in Eq. 13 is not in block-diagonal form, which is assumed in the standard μ computation. However, Eq. 16 can be easily rearranged into a standard μ problem as given in the next result.

Corollary 1. Assume that the matrix M in Figure 3 is stable. The uncertain system in this diagram is robustly stable under mixed LTI and LTV uncertainties Δ if and only if

$$\max_{\omega_1,\ \ldots,\ \omega_{n-1}} \mu_{\Delta^*}\left[\, R\tilde{M}(\omega_1,\ \ldots,\ \omega_{n-1})\, L\right] < 1,$$
$$\omega_1,\ \ldots,\ \omega_{n-1} \in [0\ \infty), \quad (18)$$

where the diagonal perturbation Δ^* is obtained by using two permutation matrices L and R as follows

$$\tilde{\Delta} = L \cdot \text{diag}\left[\, \delta_1 I_{(n-1)^2}\, \delta_2 I_{(n-1)^2} \cdots \delta_{n-1} I_{(n-1)^2}\, \delta_n I_{n-1}\right] \cdot R = L\Delta^* R, \quad (19)$$

where I_κ denotes a $\kappa \times \kappa$ identity matrix.

Note that Eq. 18 is an n-dimensional complex μ computation with repeated scalar uncertainties. Furthermore, the dimension of the matrix $R\tilde{M}L$ grows rapidly with the number of local models employed to form the global multiple model, that is, $(n-1)(n^2-2n+2)$. Coupled with the fact that $(n-1)$ frequency values are required in μ computation, Eq. 18 is not efficient from a computational point of view. Nevertheless, the results given in Theorem 2 and Corollary 1 have given us insight on the performance limitation of the IMC system given in Figure 2. In the next section, we will study a computationally efficient controller design method that originates from Corollary 1, yet offers a less conservative design method than Corollary 1.

Practical Controller Design Method

In this section we will examine closely the condition used in the description of the perturbation, Δ_i. As a result of this analysis, a controller design method that is more practical and applicable to a wider range of systems can be developed. Recall that the μ condition in Corollary 1 considers all possible combinations of perturbations whose magnitudes are not larger than one. This, however, is not the case considering the fact that the summation of all model validity functions is equal to one as given by Eq. 2. Thus, it is impossible for the values of all validity functions to approach zero simultaneously, or the values of Δ_i are not equal to -1 at the same time. Likewise, the values of all validity functions (or Δ_i for that matter) cannot reach one simultaneously. Therefore, the set of uncertainties considered in Corollary 1 is unnecessarily larger than the actual set specified by Eq. 2, thus leading to a conservative controller design method. When only two local models are used in the construction of the global model, however, Corollary 1 indeed gives a nonconservative design. This is because only one LTV uncertainty is introduced in the controller design, as shown in Eq. 12. Thus, from the point of view of controller design, it is advantageous to have a global multiple model in the following form:

$$G(\gamma^*) = \begin{cases} \gamma_1^* G_1 + (1-\gamma_1^*)G_2, & \text{if } \eta \in [\Gamma_1\ \Gamma_2] \\ \gamma_2^* G_2 + (1-\gamma_2^*)G_3, & \text{if } \eta \in [\Gamma_2\ \Gamma_3] \\ \vdots & \vdots \\ \gamma_{n-1}^* G_{n-1} + (1-\gamma_{n-1}^*)G_n, & \text{if } \eta \in [\Gamma_{n-1}\ \Gamma_n], \end{cases} \quad (20)$$

where $\gamma^* = (\gamma_1^*,\ \gamma_2^*,\ \ldots,\ \gamma_{n-1}^*)$ and η is a measurable variable that can serve as an index in the partition of the operation space. Again, the model validity function γ_i^* is bounded between 0 and 1.

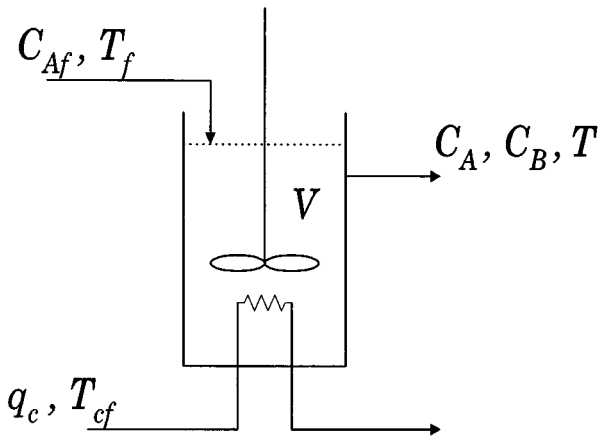

Figure 4. Continuous stirred-tank reactor.

It can be easily verified that Eq. 20 conforms to the relation in Eq. 4 and also satisfies the constraint given in Eq. 2. In other words, the model given in Eq. 20 is essentially a global multiple model with a distinct feature in that only two local models are employed to describe system dynamics. Before we present the controller design method based on the global model $G(\gamma^*)$, in the sequel we compare these two global multiple models from the point of view of modeling.

For a global multiple model comprising n local models in the operating space Γ, intuition suggests that the system dynamics at any given operating point in Γ should be approximated rather accurately by two bounding adjacent local models, that is, G_i and G_{i+1}. To illustrate this point, a continuous stirred-tank reactor (CSTR) depicted in Figure 4 is considered. It is assumed that an irreversible, first-order, exothermic reaction from component A to component B occurs in the reactor. The process is described by the following nonlinear differential equations (Lightbody and Irwin, 1995):

$$\dot{C}_A = \frac{q}{V}(C_{Af} - C_A) - k_0 C_A e^{-E/RT} \tag{21}$$

$$\dot{T} = \frac{q}{V}(T_f - T) + k_1 C_A e^{-E/RT} + k_2 q_c (1 - e^{-k_3/q_c})(T_{cf} - T), \tag{22}$$

where

$$k_1 = \frac{-\Delta H k_0}{\rho C_p} \qquad k_2 = \frac{\rho_c C_{pc}}{\rho C_p V} \qquad k_3 = -\frac{h_A}{\rho_c C_{pc}},$$

where C_A is the effluent concentration of component A, and T is the reactor temperature. The remaining model parameters and the nominal operating conditions are given in Table 1. The output and input variables are C_A and q_c, respectively.

A global multiple model using three local models is constructed first to describe the dynamics of CSTR when the operating range of C_A is $\Gamma = [0.08\ 0.12]$. These models are obtained at three operating points 0.08, 0.1, and 0.12, respectively:

Table 1. Nominal CSTR Operating Condition

Product concentration	C_A	0.1 mol/L
Reactor temperature	T	438.54 K
Coolant flow rate	q_c	103.41 L/min
Process flow rate	q	100 L/min
Feed concentration	C_{Af}	1 mol/L
Feed temperature	T_f	350 K
Inlet coolant temperature	T_{cf}	350 K
CSTR volume	V	100 L
Heat − transfer term	h_A	7×10^5 cal/min/K
Reaction-rate constant	k_o	7.2×10^{10} min^{-1}
Activation-energy term	E/R	1×10^4 K
Heat of reaction	ΔH	-2×10^5 cal/mol
Liquid densities	ρ, ρ_c	1×10^3 g/L
Specific heats	C_P, C_{PC}	1 cal/g/K

$$\Gamma_1 = 0.08: \qquad G_1 = \frac{0.0028}{0.0655s^2 + 0.3344s + 1} \tag{23}$$

$$\Gamma_2 = 0.1: \qquad G_2 = \frac{0.0037}{0.0913s^2 + 0.2439s + 1} \tag{24}$$

$$\Gamma_3 = 0.12: \qquad G_3 = \frac{0.0049}{0.1251s^2 + 0.1369s + 1}. \tag{25}$$

The associated validity functions are given as follows:

$$\Gamma_1 = 0.08: \qquad \gamma_1 = e^{-(C_A - 0.08)^2/0.008^2} \tag{26}$$

$$\Gamma_3 = 0.12: \qquad \gamma_3 = e^{-(C_A - 0.12)^2/0.015^2} \tag{27}$$

$$\Gamma_2 = 0.1: \qquad \gamma_2 = 1 - \gamma_1 - \gamma_3. \tag{28}$$

The values of γ_i are illustrated in Figure 5a. Figure 6 shows that, using these validity functions, the global multiple model can predict the actual process dynamics very well.

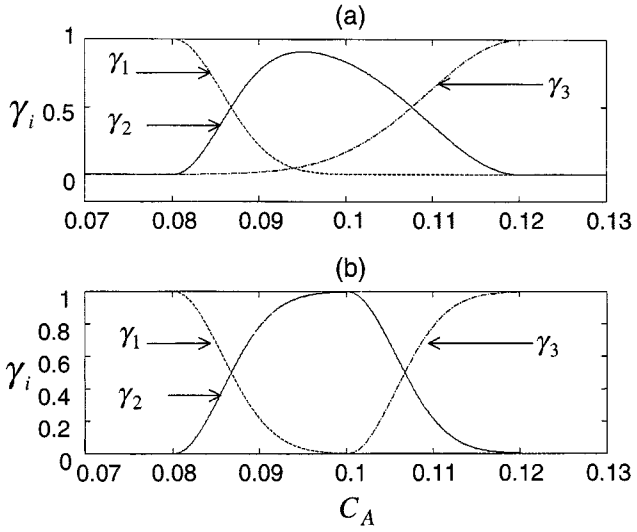

Figure 5. Validity functions of two global models.

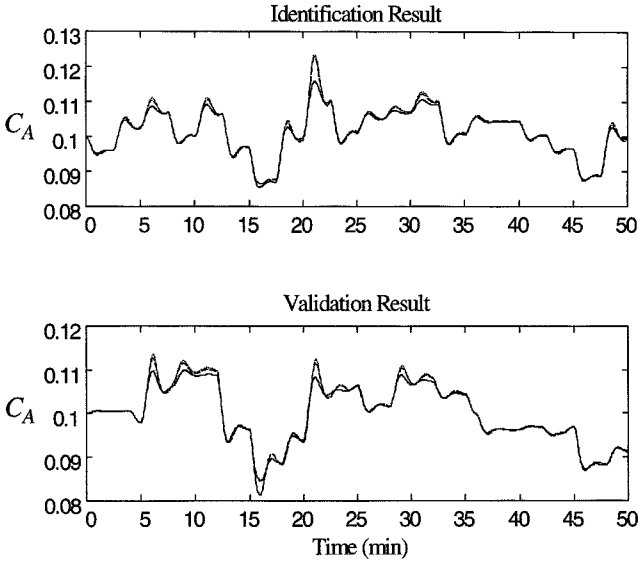

Figure 6. Modeling results: solid line—nonlinear model; dashed line—global model using Eq. 4; dotted line—global model using Eq. 20.

Next, another global multiple model using the following model validity functions is constructed:

$$\gamma_1 = \begin{cases} e^{-(C_A-0.08)^2/0.008^2} & \text{when } C_A \in [0.08,\ 0.1] \\ 0 & \text{when } C_A \in [0.1,\ 0.12] \end{cases} \tag{29}$$

$$\gamma_3 = \begin{cases} 0 & \text{when } C_A \in [0.08,\ 0.1] \\ 1 - e^{-(C_A-0.1)^2/0.008^2} & \text{when } C_A \in [0.1,\ 0.12] \end{cases} \tag{30}$$

$$\gamma_2 = \begin{cases} 1-\gamma_1 & \text{when } C_A \in [0.08\ 0.1] \\ 1-\gamma_3 & \text{when } C_A \in [0.1\ 0.12]. \end{cases} \tag{31}$$

Figure 5b gives the values of γ_i in the preceding equations. It is clear that by design, γ_1 deliberately vanishes in the operating range [0.1 0.12], whereas γ_3 is zero in the range [0.08 0.1]. As a result, only one pair of local models, (G_1, G_2) or (G_2, G_3), is employed to describe the system dynamics at any operating point in Γ. This is essentially the global model described in Eq. 20. The modeling results of this global multiple model are shown in Figure 6. It can be seen that the predictions of these two global models are very comparable. Obviously, the preceding discussion applies to n local model cases where a much finer partition is used in dividing the operating space.

Now, we proceed to develop the controller design method based on the special form of global model given in Eq. 20, from which the operating space Γ can be viewed as a union of subspace $[\Gamma_i\ \Gamma_{i+1}]$, or

$$\Gamma = \bigcup_{i=1,\ \ldots,\ n-1} [\Gamma_i\ \Gamma_{i+1}], \tag{32}$$

where two adjacent local models are used to form a global model for the respective subspace. To solve the control problem discussed in the previous section, Corollary 1 is applied repeatedly $n-1$ times to all subspaces by taking advantage of the fact that Corollary 1 is the least conservative design with two local models. In each subspace, the corresponding design constraint is as follows:

$$\mu_{\hat{\Delta}}(M_{2,i}) < 1, \qquad i = 1,\ 2,\ \ldots,\ n-1, \tag{33}$$

where

$$\hat{\Delta} = \begin{bmatrix} \delta_1 & \\ & \delta_2 \end{bmatrix}$$

and

$$M_{2,i} = \frac{1}{1+[0.5(G_i+G_{i+1})-G_M]Q} \times \begin{bmatrix} -0.5(G_{i+1}-G_i)Q & -0.5(G_{i+1}-G_i)Q \\ (1-G_MQ)W_p & (1-G_MQ)W_p \end{bmatrix}, \quad i = 1,\ 2,\ \ldots,\ n-1. \tag{34}$$

Therefore, the value of ϵ that is a solution for all subspaces gives a valid IMC design. The following corollary summarizes this result.

Corollary 2. Suppose the matrix $M_{2,i}$ in Eq. 34 is stable. The IMC structure in Figure 2 satisfies the H^∞ performance requirement if and only if μ conditions in Eq. 33 are satisfied simultaneously, that is,

$$\text{Max}\{\mu_{\hat{\Delta}}(M_{2,1}),\ \mu_{\hat{\Delta}}(M_{2,2}),\ \ldots,\ \mu_{\hat{\Delta}}(M_{2,n-1})\} < 1. \tag{35}$$

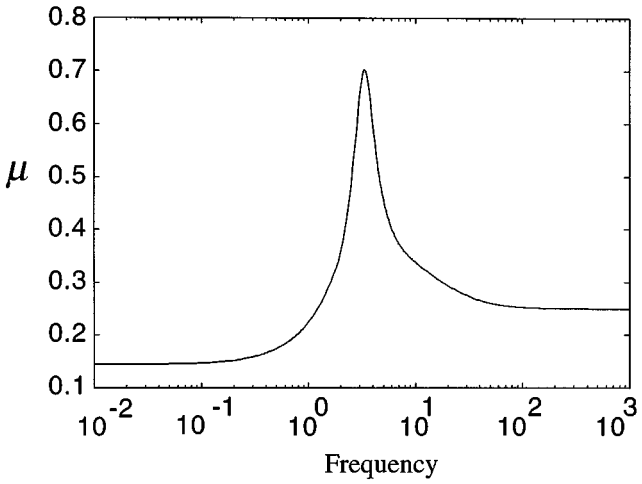

Figure 7. Robustness test of multi-model-based IMC design by Corollary 2.

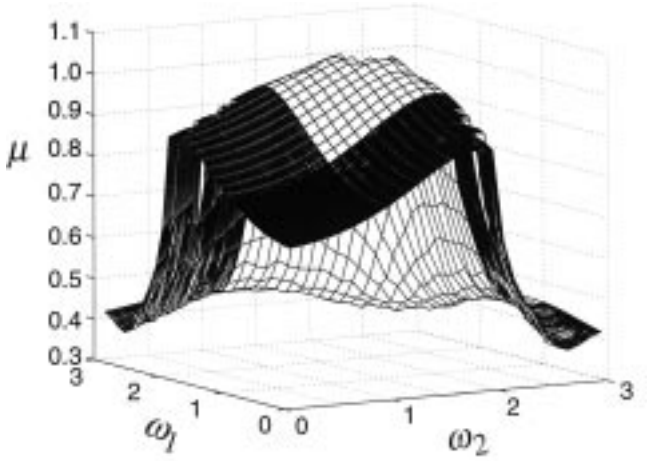

Figure 8. Robustness test of multiple-model-based IMC design by Corollary 1.

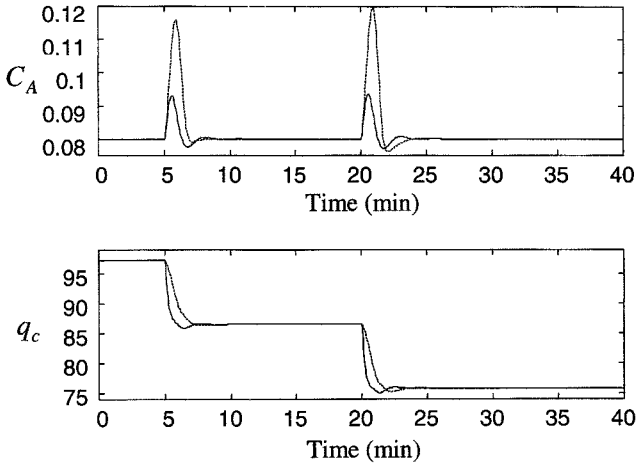

Figure 10. Closed-loop responses to step changes in T_f at operating point $C_A = 0.08$: conventional IMC design $\epsilon = 0.42$ (---), multiple-model-based design $\epsilon = 0.1$ (——).

Examples

Examples 1

The CSTR example discussed earlier is used to demonstrate the proposed IMC design procedure. The control objective is to provide a good control of C_A in the operating space [0.08 0.12] by manipulating q_c. The IMC controller is given by

$$Q = \frac{1}{G_M} \cdot \frac{1}{(\epsilon s + 1)^2}, \tag{36}$$

where G_M is the local model at the middle operating point $C_A = 0.1$ mol/L, as given in Eq. 24. The performance weight is chosen as

$$W_p = 0.25 \frac{7s + 1}{7s}. \tag{37}$$

Corollary 2 is then used to determine the value of ϵ that guarantees the H^∞ performance requirement. With IMC design $\epsilon = 0.1$, Figure 7 illustrates that the structured singular value is smaller than one; thus, Eq. 35 holds. In contrast, Eq. 16 is shown in Figure 8 for the same value of $\epsilon = 0.1$. Because the peak value is larger than one, $\epsilon = 0.1$ is not recommended by Corollary 1. Therefore, it is clear that Corollary 1 is more conservative than Corollary 2, and thus is not suitable in multiple-model-based IMC design.

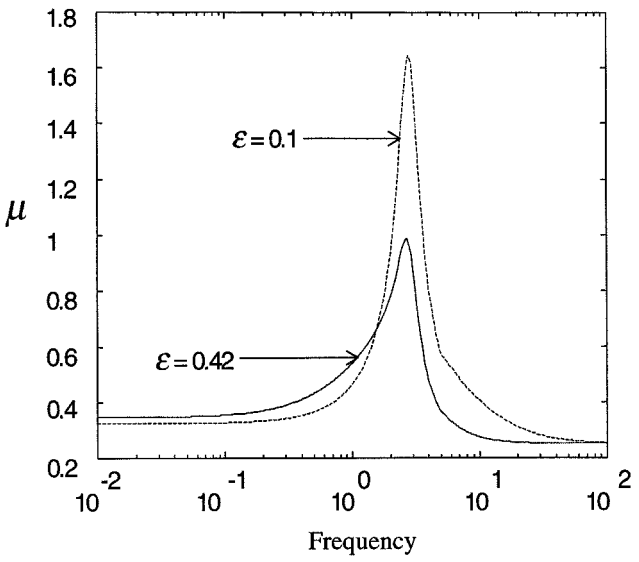

Figure 9. Robustness test of conventional IMC design.

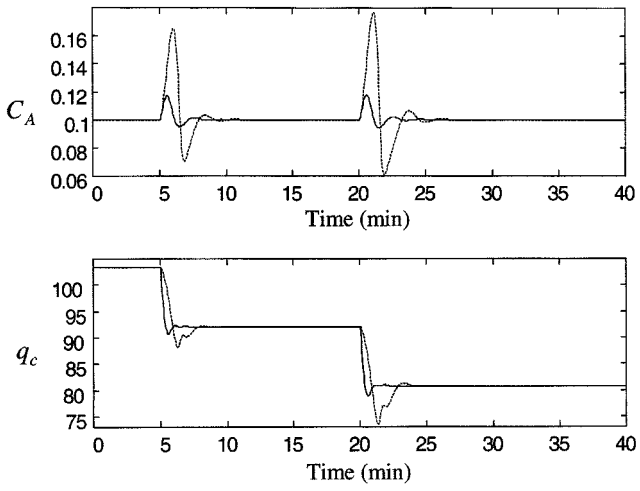

Figure 11. Closed-loop responses to step changes in T_f at operating point $C_A = 0.1$: conventional IMC design $\epsilon = 0.42$ (---), multiple-model-based design $\epsilon = 0.1$ (——).

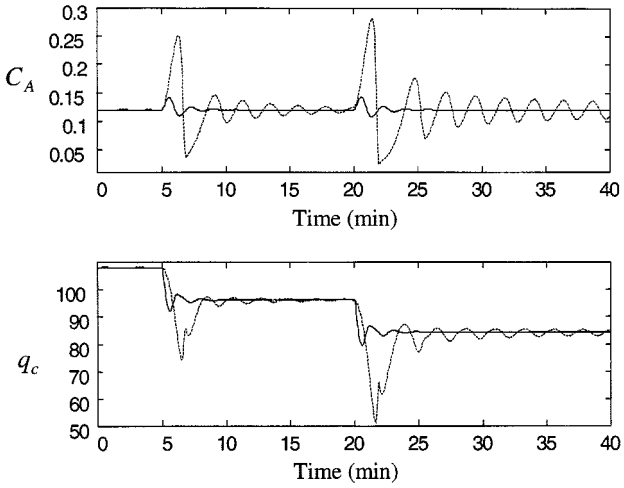

Figure 12. Closed-loop responses to step changes in T_f at operating point $C_A = 0.12$: conventional IMC design $\epsilon = 0.42$ (– – –), multiple-model-based design $\epsilon = 0.1$ (——).

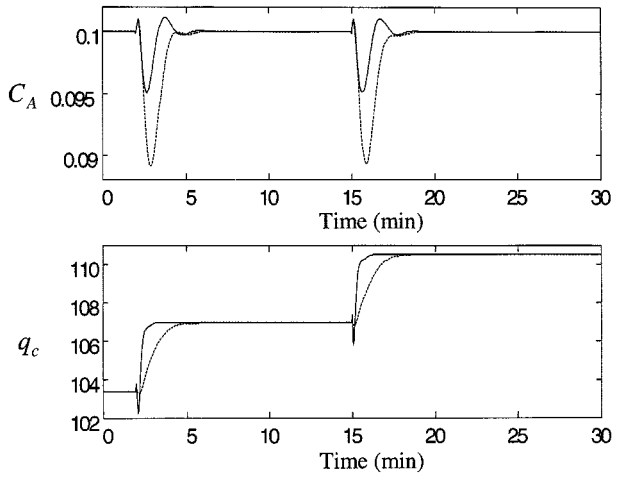

Figure 14. Closed-loop responses to step changes in C_{Af} at operating point $C_A = 0.1$: conventional IMC design $\epsilon = 0.42$ (– – –), multiple-model-based design $\epsilon = 0.1$ (——).

For comparison, the conventional IMC design is carried out to meet the same design requirement. The same IMC controller in Eq. 36 is used and the corresponding structured singular value test is shown in Figure 9, with $\epsilon = 0.1$ and 0.42. Clearly, the conventional IMC design fails to design $\epsilon = 0.1$ for this example. Figures 10 to 12 compare the regulatory responses of two controllers when successive step changes in feed temperature occur at $t = 5$ min from 350 K to 340 K and at $t = 20$ min from 340 K to 330 K, respectively. Evidently, the multiple-model-based IMC design outperforms the conventional IMC design at three operating conditions, especially at the setpoint $C_A = 0.12$ mol/L. The former design yields a much less oscillatory response and returns to the setpoint much faster than the latter design. Similar results (Figures 13 to 15) are obtained when load disturbance occurs in C_{Af} from 1 mol/L to 1.02 mol/L at $t = 3$ min, and from 1.02 mol/L to 1.04 mol/L at $t = 15$ min.

Example 2

The proposed IMC strategy is also applied to a continuous fermentor, as shown in Figure 16. The dilution rate D and the feed substrate concentration S_f are process inputs. The dilution rate is usually selected as the manipulated variable and the biomass B is a reasonable choice for the controlled output (Henson and Seborg, 1991). The fermentor is described by three nonlinear ordinary differential equations:

$$\dot{B} = -DB + \Omega B$$

$$\dot{S} = D(S_f - S) - \frac{1}{Y_{X/S}}\Omega B$$

$$\dot{P} = -DP + (\alpha\Omega + \beta)B, \tag{38}$$

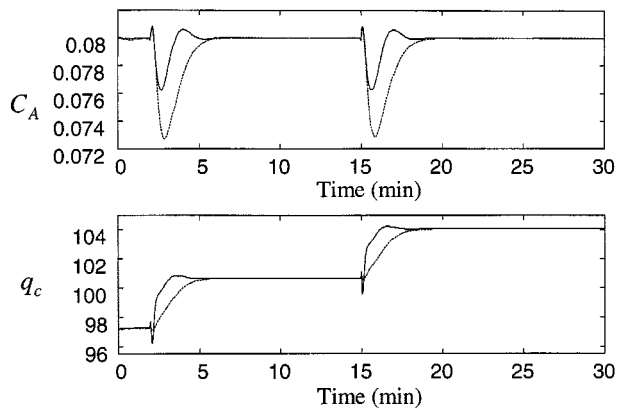

Figure 13. Closed-loop responses to step changes in C_{Af} at operating point $C_A = 0.08$: conventional IMC design $\epsilon = 0.42$ (– – –), multiple-model-based design $\epsilon = 0.1$ (——).

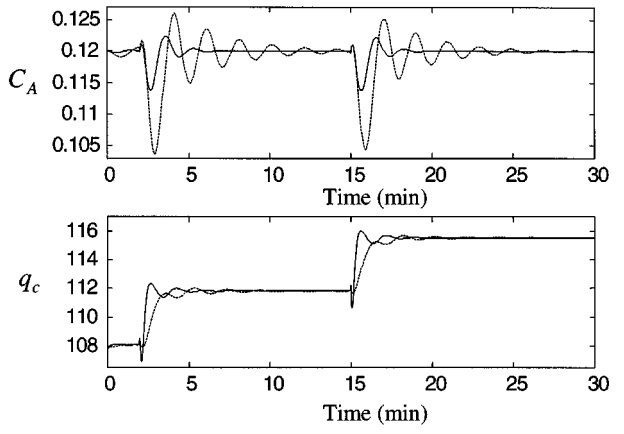

Figure 15. Closed-loop responses to step changes in C_{Af} at operating point $C_A = 0.12$: conventional IMC design $\epsilon = 0.42$ (– – –), multiple-model-based design $\epsilon = 0.1$ (——).

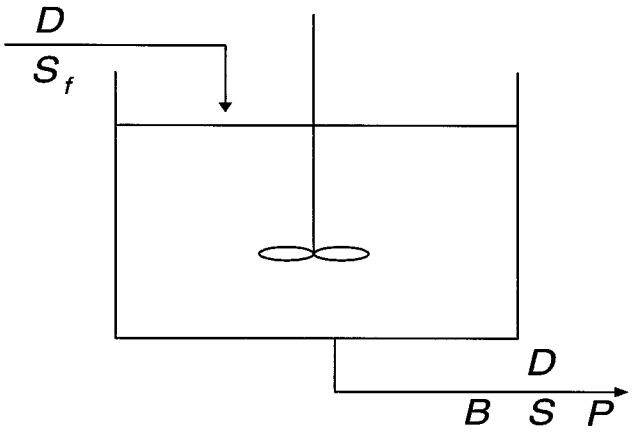

Figure 16. Continuous fermentor.

where S is the substrate concentration, P is the product concentration, Ω is the specific growth rate, $Y_{X/S}$ is the cell-mass yield, and α and β are kinetic parameters. The specific growth rate has the following form:

$$\Omega = \frac{\Omega_m\left(1-\frac{P}{P_m}\right)S}{K_m + S + \frac{S^2}{K_i}} \tag{39}$$

where Ω_m is the maximum specific growth rate, P_m is the product saturation constant, K_m is the substrate saturation constant, and K_i is the substrate inhibition constant. Nominal parameters and operating conditions (Henson and Seborg, 1991) used for the simulations are listed in Table 2.

Suppose that the fermentor operates in the range of (5, 7), three local models are constructed first, as follows:

$$B = 5 \qquad G_1 = \frac{-5s^2 - 2.06s - 0.21}{s^3 + 0.47s^2 + 0.07s + 0.0027} \tag{40}$$

$$B = 6 \qquad G_2 = \frac{-6s - 2.19s - 0.20}{s^3 + 0.50s^2 + 0.09s + 0.0053} \tag{41}$$

$$B = 7 \qquad G_3 = \frac{-7s^2 - 1.76s - 0.11}{s^3 + 0.65s^2 + 0.14s + 0.0093}. \tag{42}$$

Table 2. Nominal Fermentor Operating Conditions

$Y_{X/S}$	0.4	g/g	K_i	22	g/L
α	2.2	g/g	S_f	20	g/L
β	0.2	h^{-1}	D	0.202	h^{-1}
Ω_m	0.48	h^{-1}	B	6.0	g/L
P_m	50	g/L	S	5.0	g/L
K_m	1.2	g/L	P	19.14	g/L

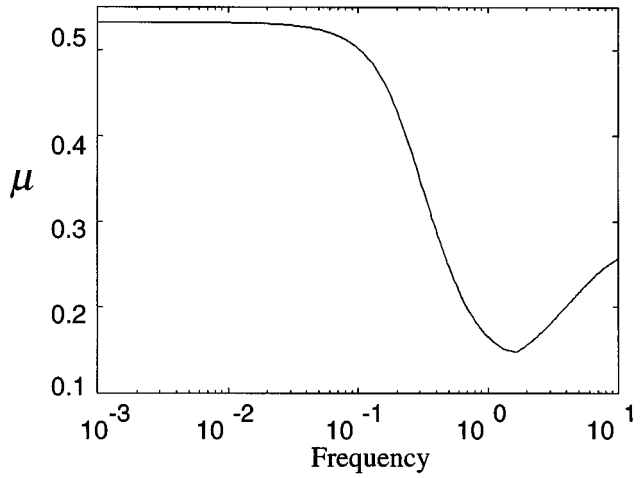

Figure 17. Robustness test of multiple-model-based IMC design by Corollary 2.

The IMC controller is designed to be

$$Q = G_3^{-1}\frac{1}{\epsilon s + 1}. \tag{43}$$

With the same performance weight given in Eq. 37 and $\epsilon = 0.1$, Figure 17 shows that Eq. 35 is satisfied with this IMC design. Again, the conservativeness of Corollary 1 is verified by Figure 18, where Eq. 16 is not satisfied with $\epsilon = 0.1$.

It is noted, however, that the conventional IMC design will fail by using the preceding three local models, because it is natural to choose operating point $B = 6$ g/L as the nominal model, and treat the other two operating points as the perturbed processes. In doing so, however, the gain changes between the nominal model, and the perturbed model at $B = 5$ g/L will be more than 100%. Consequently, the conventional

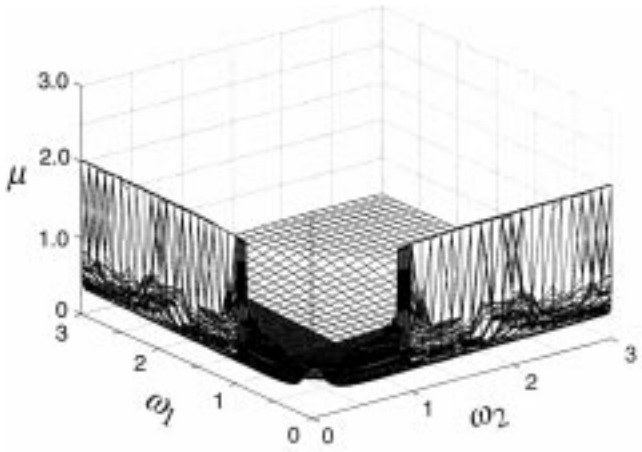

Figure 18. Robustness test of multiple-model-based IMC design by Corollary 1.

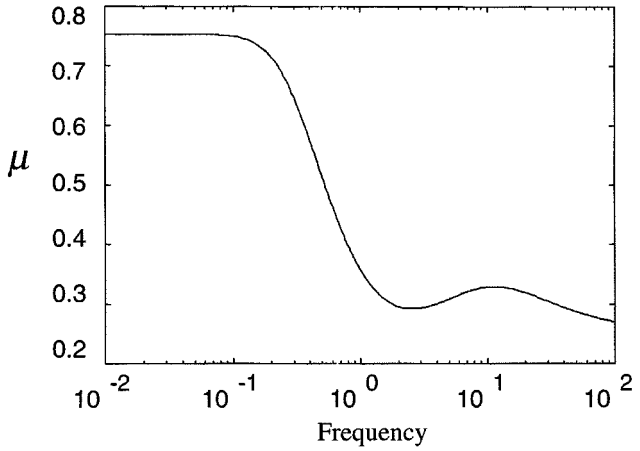

Figure 19. Robustness test of conventional IMC design.

IMC design cannot satisfy this design requirement (Morari and Zafiriou, 1989).

To overcome this limitation, the following local model is deliberately chosen so that the conventional IMC design is feasible

$$B = 5.7718 \qquad G_0 = \frac{-5.7718s^2 - 2.1849s - 0.2049}{s^3 + 0.4841s^2 + 0.0793s + 0.0045}. \quad (44)$$

Next, the IMC controller is designed as

$$Q = G_0^{-1}\frac{1}{\epsilon s + 1}. \quad (45)$$

Figure 19 shows that the robustness test is satisfied with $\epsilon = 0.1$. Figure 20 illustrates that these two IMC designs exhibit similar servo responses. Figures 21 to 23 compare the closed-loop responses of two controllers to an unmeasured step disturbance of -0.08 in Ω_m. Clearly, the proposed IMC

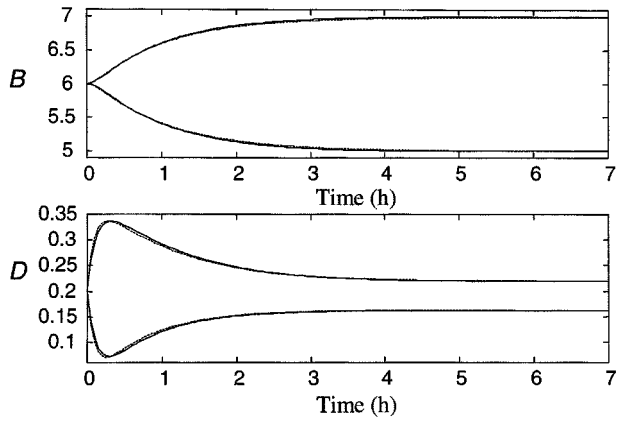

Figure 20. Set point change responses: conventional IMC $\epsilon = 0.1$ (---), multiple-model-based design $\epsilon = 0.1$ (——).

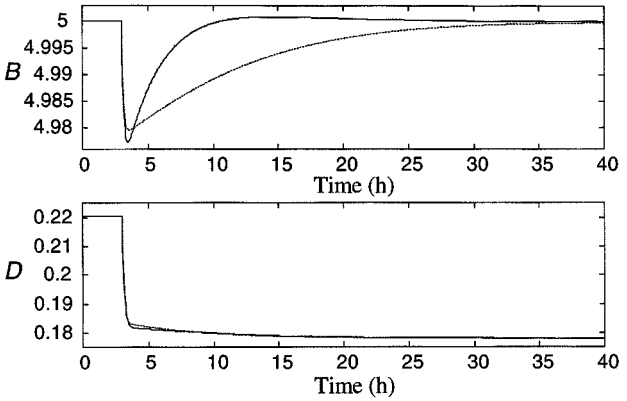

Figure 21. Closed-loop responses to step changes in Ω_m at operating point $B = 5$: conventional IMC $\epsilon = 0.1$ (---), multiple-model-based design $\epsilon = 0.1$ (——).

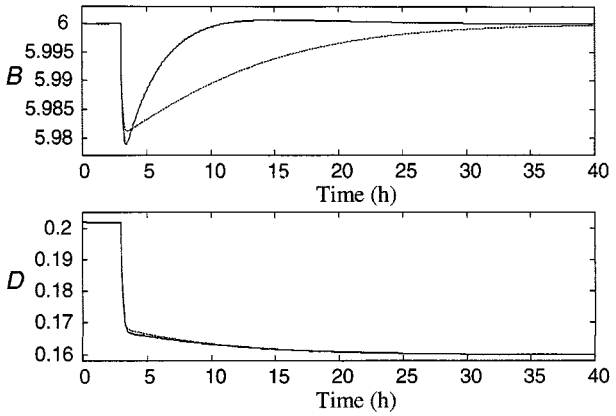

Figure 22. Closed-loop responses to step changes in Ω_m at operating point $B = 6$: conventional IMC $\epsilon = 0.1$ (---), multiple-model-based design $\epsilon = 0.1$ (——).

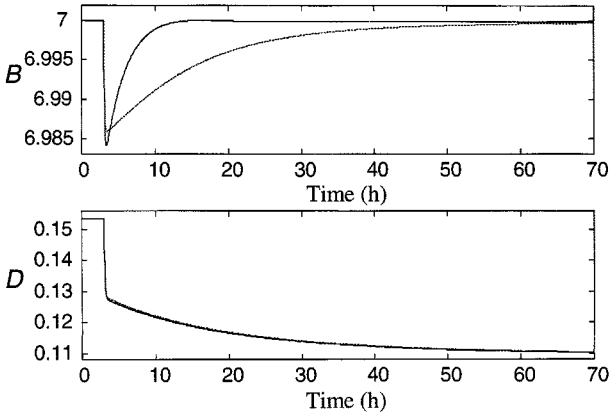

Figure 23. Closed-loop responses to step changes in Ω_m at operating point $B = 7$: conventional IMC $\epsilon = 0.1$ (---), multiple-model-based design $\epsilon = 0.1$ (——).

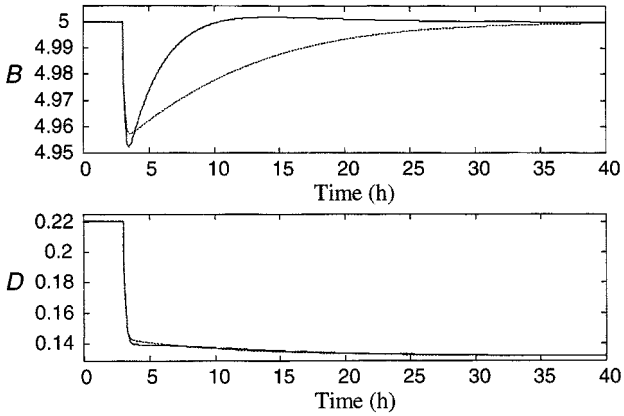

Figure 24. Closed-loop responses to step changes in K_i at operating point $B = 5$: conventional IMC $\epsilon = 0.1$ (– – –), multiple-model-based design $\epsilon = 0.1$ (——).

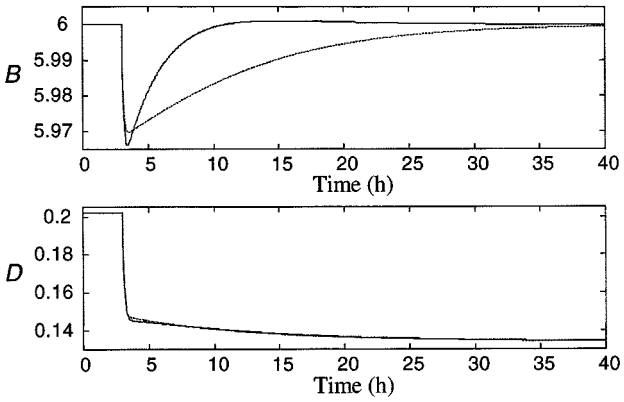

Figure 25. Closed-loop responses to step changes in K_i at operating point $B = 6$: conventional IMC $\epsilon = 0.1$ (– – –), multiple-model-based design $\epsilon = 0.1$ (——).

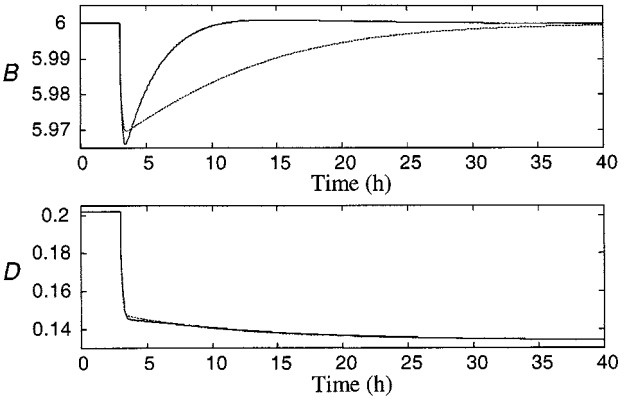

Figure 26. Closed-loop responses to step changes in K_i at operating point $B = 7$: conventional IMC $\epsilon = 0.1$ (– – –), multiple-based design $\epsilon = 0.1$ (——).

design achieves a faster response than the conventional IMC design. For the unmeasured step disturbance of -15.4 in K_i, a similar conclusion is also observed in Figures 24 to 26.

Conclusions

A novel IMC design method is proposed to address the H^∞ performance of dynamics systems operated over a range of operating points. The main idea is to construct a set of local transfer-function models to represent the dynamic system around each operating point, and then to connect the set of local models by validity functions to form a global dynamic model. Subsequently, the global model can be recast as an uncertain system with bounded LTI and LTV perturbations. An augmented μ design method is used to analyze the resulting H^∞ control problem. Simulation results demonstrate the advantages of the proposed IMC design over its conventional counterpart.

Notation

G_M = local model for IMC controller design
G_i = ith local model of the global multiple-model system
U = input variable of the system
Y_i = local output variable of the system
δ_i = ith perturbation
Δ = block diagonal perturbation matrix
Δ_i = fictitious uncertainty block associated with weighting function
Δ_{ii} = diagonal uncertainty in the augmented uncertainty block $\tilde{\Delta}$
ω = frequency

Literature Cited

Banerjee, A., Y. Arkun, B. Ogunnaike, and R. Pearson, "Estimation of Non-Linear Systems Using Linear Multiple Models," *AIChE J.*, **43**, 1204 (1997).

Doyle, J. C., "Analysis of Control Systems with Structured Uncertainty," *IEEE Proc., Part D*, **129**, 242 (1982).

Feng, G., S. G. Cao, and N. W. Rees, "An Approach to H^∞ control of a Class of Nonlinear Systems," *Automatica*, **32**, 1469 (1996).

Henson, M. A., and D. E. Seborg, "An Internal Model Control Strategy for Nonlinear Systems," *AIChE J.*, **37**, 1065 (1991).

Johansen, T. A., and B. A. Foss, "Constructing NARMAX Models Using ARMAX Models," *Int. J. Control*, **58**, 1125 (1993).

Johansen, T. A., and B. A. Foss, "Operating Regime Based Process Modeling and Identification," *Comput. Chem. Eng.*, **21**, 159 (1997).

Lightbody, G., and G. W. Irwin, "Direct Neural Model Reference Adaptive Control," *IEE Proc., Part D*, **142**, 31 (1995).

Morari, M., and E. Zafiriou, *Robust Process Control*, Prentice Hall, Englewood Cliffs, NJ (1989).

Packard, A., and J. Doyle, "The Complex Structured Singular Value," *Automatica*, **29**, 71 (1993).

Paganini, F., "Robust Stability Under Mixed Time-Varying, Time-Invariant and Parametric Uncertainty," *Automatica*, **32**, 1381 (1996).

Palizban, H. A., A. A. Safari, and J. A. Romagnoli, "A Nonlinear Controller Design Approach Based on Multi-Linear Models," *Proc. ACC*, Army Chemical Center, 3490 (1997).

Poolla, K., and A. Tikku, "Robust Performance Against Time-Varying Structured Perturbations," *IEEE Trans. Automat. Contr.*, **AC-40**, 1589 (1995).

Pottmann, M., H. Unbehauen, and D. E. Seborg, "Application of a General Multi-Model Approach for Identification of Highly Nonlinear Processes—a Case Study," *Int. J. Control*, **57**, 97 (1993).

Shamma, J. S., "Robust Stability with Time-Varying Structured Uncertainty," *IEEE Trans. Automat. Contr.*, **AC-39**, 714 (1994).

Takagi, T., and M. Sugeno, "Fuzzy Identification of Systems and Its Applications to Modeling and Control," *IEEE Trans. Syst. Man, Cybern.*, **SMC-15**, 116 (1985).

Appendix A: Proof of Theorem 1

Rearranging Eq. 5 gives

$$\left|\frac{G}{G_M}-1\right|\le|l_1|,\qquad G\in\{G_1, G_2, \ldots, G_n\},\qquad \forall\omega. \quad \text{(A1)}$$

Therefore, at each frequency, the tightest bound of $|l_1|$ is calculated by

$$\operatorname*{Max}_{G}\left|\frac{G}{G_M}-1\right|=|l_1|,\qquad G\in\{G_1, G_2, \ldots, G_n\}. \quad \text{(A2)}$$

Similarly, Eq. 6 yields

$$\operatorname*{Max}_{\gamma_i}\left|\frac{\sum_{i=1}^{n}\gamma_i G_i}{G_M}-1\right|=|l_2|. \quad \text{(A3)}$$

It then can be derived that

$$\left|\frac{\sum_{i=1}^{n}\gamma_i G_i}{G_M}-1\right|=\left|\frac{\sum_{i=1}^{n}\gamma_i(G_i-G_M)}{G_M}\right|\le\sum_{i=1}^{n}\gamma_i\left|\frac{G_i}{G_M}-1\right|$$

$$\le\sum_{i=1}^{n}\gamma_i|l_1|=|l_1|. \quad \text{(A4)}$$

Combining Eqs. A3 and A4 completes the proof.

Appendix B: Derivation of the Matrix *M* in Figure 3

From Figure 2, it can be derived that

$$e=y'-y=G_M Qe-y=\frac{-y}{1-G_M Q}, \quad \text{(B1)}$$

since

$$y=G_1 Qe+\sum_{2}^{n}v_i+0.5Q\sum_{2}^{n}\Delta G_i e+v_p. \quad \text{(B2)}$$

Substituting Eq. B1 into Eq. B2 gets

$$y=\frac{1-G_M Q}{1+(G_1-G_M)Q+0.5Q\sum_{2}^{n}\Delta G_i}\left(\sum_{2}^{n}v_i+v_p\right). \quad \text{(B3)}$$

Therefore

$$u_p=W_p y=\frac{(1-G_M Q)W_p}{1+(G_1-G_M)Q+0.5Q\sum_{2}^{n}\Delta G_i}\left(\sum_{2}^{n}v_i+v_p\right) \quad \text{(B4)}$$

and

$$u_i=0.5\Delta G_i Qe=\frac{-0.5\Delta G_i Q}{1+(G_1-G_M)Q+0.5Q\sum_{2}^{n}\Delta G_i}\left(\sum_{2}^{n}v_i+v_p\right),\qquad i=2, 3, \ldots, n. \quad \text{(B5)}$$

Finally, the matrix M in Figure 3 can be obtained from both Eqs. B4 and B5. The proof is complete.

Manuscript received Sept. 14, 1998, and revision received July 26, 1999.